Contrib. Astron. Obs. Skalnaté Pleso **33**, 209 – 223, (2003)

The influence of a coronal inhomogeneity on emission spectral line intensities and on coronal iron abundance determination

P. Schwartz

Astronomical Institute, Academy of Sciences of the Czech Republic, 25165 Ondřejov, Czech Republic
(E-mail: schwartz@asu.cas.cz)

Received: July 1, 2001

Abstract. The aim of this paper is to show how much coronal inhomogeneity could influence emission line intensities and iron abundance determination using these intensities. Although the latest methods can consider temperature changes along the line of sight, presence of areas with very different electron densities cannot be taken into account. We argue that in case the line of sight goes through some coronal inhomogeneity, iron abundance determination from emission lines intensity using the present methods could differ up to 2 orders of magnitude from the actual value. A new method is suggested in this paper which should solve not only the problem of the iron abundance determination in the solar corona but it could help in electron density and temperature determination in coronal inhomogeneity as well.

Key words: Sun – corona – emission lines – iron abundance

1. Introduction

There are still problems of determination of the iron abundance in the solar corona using emission spectral lines photometry. Not only the green and red coronal line intensities but many other fainter lines of different iron ions are needed for a reliable iron abundance determination. But a majority of other coronal spectral lines of iron ions are measurable only in places with a suitable electron density and temperature. A particular structure in the solar corona, radiating in many spectral lines of iron ions at the same time with measurable intensities, must consist of many areas with very different electron densities and temperatures. Such a structure is named hereafter a coronal inhomogeneity because it differs from the quiet corona background.

Nowadays there are more advanced techniques using a differential emission measure (DEM) (Mason et al., 1999). They can solve multitemperature problem, but they are not capable of taking into account changes of electron densities along the line of sight (Landi and Landini, 1997). These changes could be significant when there are inhomogeneities along the line of sight. Electron density

inside a coronal inhomogeneity can be up to 10 times greater than in the surrounding corona (Mason, 1975). Therefore, emission spectral lines of some ions can be more intense in the area where an inhomogeneity is present than in the corona outside the inhomogeneity. Thus one could determine wrong value of the coronal iron abundance having assumed a spherical symmetry for electron density and temperature distribution. The value of coronal abundance of iron 7.2×10^{-5} determined by Pottasch (1963) was almost 20 times greater than the photospheric one determined by Goldberg et al. (1960) from the curve of growth. But the photospheric iron abundance value given by Goldberg et al. (1960) is very different from the average meteoritic iron abundance in carbonous chondrites 3.24×10^{-5} (Anders and Grevesse, 1989). Carbonous chondrites are thought as a sample of original matter (besides volatile materials) from which the solar system and Sun were formed.

From the beginning of the 70th of the last century, values of photospheric iron abundance estimated by various authors are close to the recent value of photospheric iron abundance 3.16×10^{-5} (Grevesse and Sauval, 1999). This value is much closer to the meteoritic one than Goldberg's one. It is determined not using a curve of growth and equivalent widths, but profiles of faint FeI spectral lines are fitted by synthetic spectrum. However, Pottasch's iron abundance in the solar corona is 2.28 times larger than the photospheric one determined by Grevesse and Sauval (1999). The value of photospheric iron abundance estimated by Goldberg et al. (1960) is by an order lower than values of other authors because of very inaccurate computations of oscillator strengths for FeI photospheric spectral lines (Grevesse and Sauval, 1999).

It is true that measurements (from eclipses during 1949 – 1954) which Pottasch used for his analysis are not very suitable for the determination of iron abundances because they were made in different times and at different positions in the solar corona. Although Pottasch selected only measurements of quiet areas, it is known that physical conditions and magnetic activity manifestations in the solar corona have strong relations to the phase of a solar cycle. The influence of an inhomogeneity on intensity is even larger than the influence of solar cycle as it is evident from section 3.

Mason (1975) tried to recompute the iron abundance from data used by Pottasch using new more accurate atomic parameters for excitation and ionization equilibrium. The value 7.0×10^{-5} determined by her does not differ much from Pottasch's one, so atomic parameters did not influence iron abundance so much.

The average abundance of iron was determined by Fludra and Schmelz (1999) from observation of 57 flares using DEM. They used data obtained by the BCS spectrometer on-board of YOHKOH. Their results show greater scatter about the mean value 4.5×10^{-5} ($\pm 1.3 \times 10^{-5}$). This mean value is 1.42 times greater than the photospheric value reported by Grevesse and Sauval (1999). Thus there is still problem why the coronal abundance of iron is different from the photospheric one or whether there is any difference at all.

There are two empirical models for a coronal-to-photospheric abundance ratio according to First Ionization Potential (FIP).

First model presumes that the low-FIP elements (FIP less then 10 eV) are 3 times more abundant in the slow solar wind (Peter, 1998a) than in the photosphere and the high-FIP elements have the same abundance in the corona as in the photosphere. In the fast solar wind low-FIP elements are only below 2 times overabundant. This model is supported especially by the solar energetic-particle data (SEP) (Feldman, 1992, Meyer, 1993). SEP is the material escaped out from corona. This material is influenced by processes of diffusion and photoionization in the chromosphere and therefore the low-FIP elements can be overabundant. The low-FIP elements have short ionization times and are coupled quickly to the solar wind flow of the main gas – ionized hydrogen while the high-FIP elements remain longer in the neutral phase (Peter, 1998b). That is why the low-FIP elements are enriched in the solar wind.

Second model is based on the assumption that the low-FIP elements have the same abundance in the corona and in the photosphere and the high-FIP elements are 4 times less abundant in corona than in photosphere. This model is supported especially by spectroscopic measurements (Meyer, 1996). From X--ray spectroscopy of solar flares it was assumed that the coronal-to-photospheric ratio of iron abundance should not be greater then 2 (Philips et al., 1994).

Therefore abundance values of elements in the solar corona should be somewhere between predictions of the above two models.

FIP of iron is about 8 eV so iron belongs to the low-FIP elements. Most of iron abundance values lie between predictions of those two empirical models described above, so the coronal iron abundance determination is not still fixed. In this paper we test an influence of inhomogeneities on coronal line intensity assuming the iron abundance to be constant.

We decided to solve such a theoretical problem because the corresponding information is important for determination of the iron abundance from emission line intensities emitted from the solar corona above an active region. Such a test could also indicate an error of the abundance determination if presence of inhomogeneity was neglected.

Simplified models of inhomogeneity used in this paper are shown in section 2, in section 3 emission line intensity computations are briefly described. Resulting intensity relations to height above the limb both in the cases with and without the inhomogeneity are shown in section 4. A method for iron abundance determination, overcoming the problem of coronal inhomogeneity presence, is outlined in section 5. The results are discussed in section 6.

2. Simplified models of the inhomogeneity

Three cases of models have been selected for mutual comparison (see Fig. 1). First one contains no inhomogeneity in the corona having classical spherical sym-

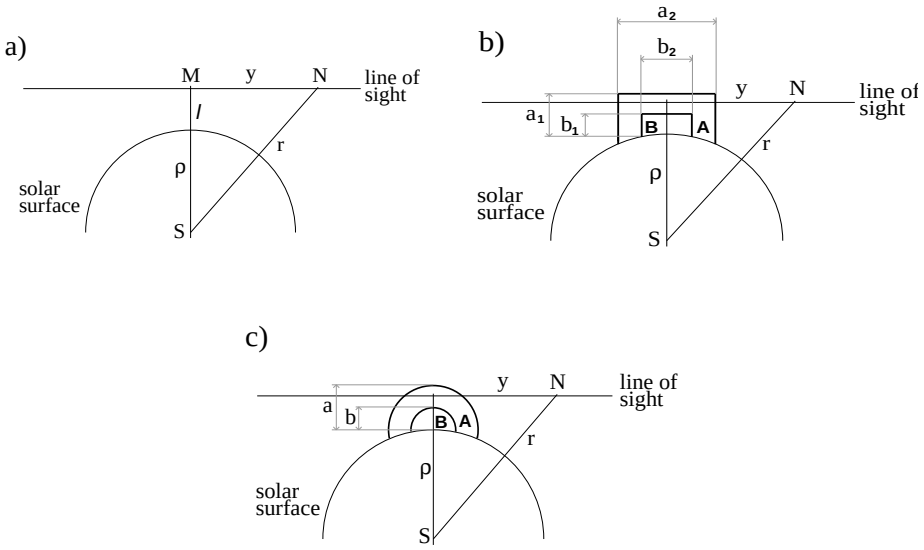

Figure 1. Three model cases, for which intensities were computed. Case `a)` without any inhomogeneity. The line of sight is going through the corona at a height l above limb (distance between the solar surface and the point M). Case `b)` with a two-component rectangular box-shaped inhomogeneity. The dimensions of boxes A,B are: $a_1 = 0.093\ R_\odot$, $a_2 = 0.36\ R_\odot$, $b_1 = 0.074\ R_\odot$, $b_2 = 0.20\ R_\odot$. Case `c)` with a two-component round-shaped (loop-like) inhomogeneity. The radii of loops A,B are: $a = 0.09\ R_\odot$, $b = 0.07\ R_\odot$.
ρ is the distance between the point M and the center of the Sun (S), so it is the distance between the center of the solar disk and position of observation, when the solar corona is projected on the sky as a two-dimensional object. Point N is at some location on the line of sight. For spectral line intensity evaluation (integrating along y) N is moving along the whole line of sight. r is the distance between place in the solar corona marked N and center of the Sun (point S). $r^2 = \rho^2 + y^2$ and $\rho = R_\odot + l$.

metry. Two other models correspond to different shapes of the inhomogeneities placed in the corona above the solar limb. Case `a)` is without any inhomogeneity, so intensity could be computed assuming spherical symmetry (Fig. 1a). We adopted a common assumption that the distribution of electron density is a spherically symmetric in the case `a)` and this distribution has been taken from measurements of Doschek et al. (1997). These authors determined electron density from the ratio of two emission lines of Si VIII (λ144.576 nm and λ144.076 nm) using the SoHO/SUMER measurements made on November 20 and December 10, 1996 nearby a southern coronal hole. Electron density varied

Table 1. Coronal emission spectral lines in the visible range of spectrum of different iron ions used in this paper.

ion	central wavelength λ_o [nm]	configuration transition	$i_\odot(\lambda_o)$ $\left[\mathrm{W\,cm^{-2}sr^{-1}\AA^{-1}}\right]$	line formation temperature $\log T$
FeIX	435.9	$3p^5 3d$ $^3\mathrm{F}_2$–$^1\mathrm{D}_2$	0.46	5.80
FeX	637.4	$3s^2 3p^5$ $^2\mathrm{P}_{3/2}$–$^2\mathrm{P}_{1/2}$	0.30	6.00
FeXI	398.7	$3s^2 3p^4$ $^3\mathrm{P}_1$–$^1\mathrm{D}_2$	0.46	6.09
FeXIV	530.3	$3s^2 3p$ $^2\mathrm{P}_{1/2}$–$^2\mathrm{P}_{3/2}$	0.38	6.30
FeXV	705.86	$3s\,3p$ $^3\mathrm{P}_1$–$^3\mathrm{P}_2$	0.23	6.30

from 5.71×10^7 cm^{-3} at the height of 0.05 $R_\odot$ above the limb to 4.06×10^6 cm^{-3} at 0.3 $R_\odot$. Temperature 1.5×10^6 K was adopted to be constant for heights up to 0.3 $R_\odot$ above the limb. Case `b)` is proposed with a two-component rectangular inhomogeneity (Fig. 1b) of typical sizes for a coronal condensation (Mason, 1975). In area A the electron density is 10^9cm^{-3} and the temperature is 2×10^6K. More dense area B has electron density $n_\mathrm{e} = 10^{10}$cm^{-3} and the temperature T_e is equal to 5×10^6 K. Outside the inhomogeneity temperature and electron density distributions are identical with those adopted for case `a)`. Case `c)` has a round (loop-like) inhomogeneity (Fig. 1c). It has two areas A and B with the same physical conditions as in the case `b)`. Sizes for this inhomogeneity were chosen in order to have the same heights of areas A and B as in case `b)`. Outside this inhomogeneity the physical conditions are again the same as in case `a)`.

3. Intensities of emission spectral lines

Five coronal emission spectral lines of different iron ions in the visible range of spectrum (listed in Table 1) were used for our theoretical model. In the first column of this table iron ions, in second column central wavelengths λ_o and in the third column transitions are listed for spectral lines of our interest. In the 4th column spectral intensities of solar disk centre at wavelengths λ_o corrected

for photospheric absorption lines are listed (Neckel and Labs, 1984, 1985). In the last column are listed line formation temperatures determined from data of excitation and ionization equilibrium used in this paper.

The solar corona is optically thin for these spectral lines. So the spectral intensity at the wings of the spectral line is small compared to the spectral line core. Therefore, we could neglect contribution of wings and compute integral intensities only for cores of spectral lines. Integral intensities of emission lines were computed by integration of emission along the whole line of sight. Practically we integrated numerically to the both sides from point M (see Fig. 1) up to points on line of sight with $r = 1.3\ R_\odot$. There was contribution to the intensity already less than 10^{-8} % of maximal value of emission on the line of sight. So we could compute integral intensity of the coronal emission spectral line at height l from range $0.05\,R_\odot - 0.15\,R_\odot$ using equation:

$$I = \frac{h\ c\ A(\mathrm{Fe})\ A_{ul}}{4\pi\lambda_\mathrm{o}} \int_{-\infty}^{\infty} \frac{N(H)}{n_\mathrm{e}}\, f(n_\mathrm{e}, T)\, g(T)\, n_\mathrm{e}\ dy \tag{1}$$

where h is Planck's constant, c velocity of light in vacuum, A_{ul} Einstein's coefficient of spontaneous emission, λ_o central wavelength of emission line. $A(\mathrm{Fe})$ is the abundance of iron in the solar corona (relative to the hydrogen concentration) and the value 4.5×10^{-5} (Fludra and Schmelz, 1999) has been taken. Ratio $f(n_\mathrm{e}, T) = \frac{N_u}{N(ion)}$ is both electron density and temperature dependent. It is the fraction of ion concentration in upper level of transition N_u to total ion number $N(ion)$. One can obtain this ratio solving equations of the excitation equilibrium. The atomic database CHIANTI (Landi et al., 1999) has been used for that reason. Routines for computing the level populations (provided in CHIANTI) were slightly changed to account for a relation to the dilution factor which varies with height above the limb.

Ratio $g(T) = \frac{N(ion)}{N(\mathrm{Fe})}$ is a temperature dependent fraction of ion concentration to concentration of all iron. This fraction results from the ionization equilibrium. Results of ionization equilibrium for iron ions using Maxwellian distribution have been taken from paper of Dzifčáková (1998). Defining $G(n_\mathrm{e}, T) = f(n_\mathrm{e}, T)\ g(T)$ and assuming $\frac{N(\mathrm{H})}{n_\mathrm{e}}$ to be constant value 0.833 (Pottasch, 1963), the equation (1) can be written in the form:

$$I = \mathrm{C} \int_{-\infty}^{\infty} G(n_\mathrm{e}, T)\, n_\mathrm{e}\, dy \tag{2}$$

where C is a constant. It is integrated along the whole line of sight at different heights l (see figures 1 a – c) so it is needed to know how $G(n_\mathrm{e}, T)$ and n_e change along the line of sight. Those quantities are spherically distributed in case `a)` along the whole line of sight and in cases `b)`, `c)` in parts outside of the inhomogeneity. In the cases of an inhomogeneity it is needed to know how long the parts of the line of sight going through areas A and B in the inhomogeneity are. Getting these quantities, the integral along the whole line of sight can be computed.

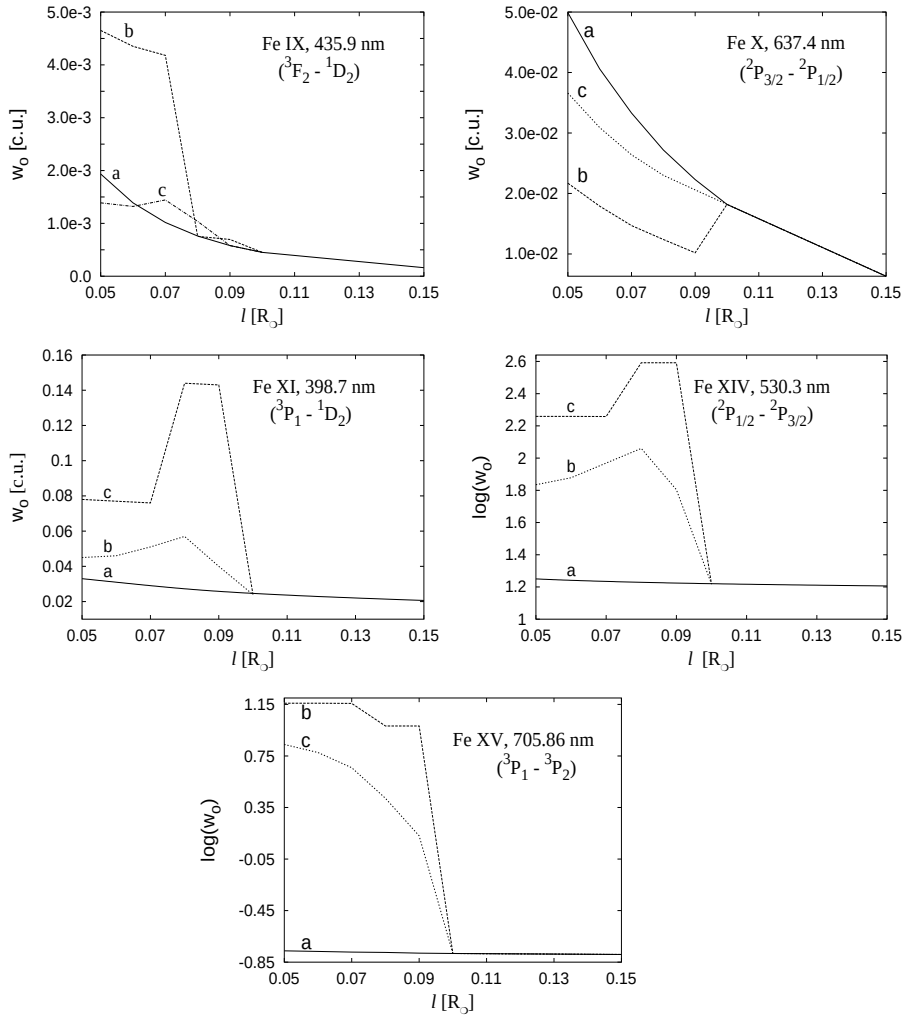

Figure 2. Relation of the equivalent widths w_o to height l above the limb for all investigated emission spectral lines (listed in table 1 in section 3) for cases `a)`, `b)` and `c)`. Equivalent widths w_o are expressed in coronal units (*c.u.*) where 1 *c.u.* $= 10^{-6}$Å. We used $\log(w_o)$ instead of w_o in graphs for lines FeXIV 530.3 nm and FeXV 705.86 nm because of large differences between equivalent widths for case `a)` and cases `b)`, `c)`.

4. Results

Our theoretical models result in intensities of different iron lines in cases without and with an inhomogeneity. Then the iron abundance neglecting inhomogenei-

ty is computed. Error which could arise in the iron abundance determination having neglected an inhomogeneity is discussed.

4.1. Intensities

Relations of the emission line equivalent width $w_o = \frac{I}{i_\odot(\lambda_o)}$ to the height above the limb l are presented here for all investigated emission lines listed in section 3 and for all three model cases (Fig. 2). The equivalent widths w_o were used instead of integral intensities because they are more common in the literature and thus easy to use for a comparison.

Significant differences can be seen between equivalent width relations to height above the limb (hereafter relations) for case `a)` and for cases `b)`, `c)` for heights smaller than 0.1 $R_\odot$. For larger heights all three equivalent width relations are the same because the height of an inhomogeneity is just 0.1 $R_\odot$ for both cases `b)` and `c)` (see figures 1a–b). For case `a)` equivalent widths of all emission lines presented here are declining exponentially with height above the limb. Differences between equivalent width relations in case without and in cases with inhomogeneity are due to substantially different physical conditions. That means when one would measure spectral line intensity at a place in the solar corona where an inhomogeneity is present, the line of sight goes through the areas with very different temperatures and electron densities.

For FeIX 435.9 nm, FeXI 398.7 nm and FeXIV 530.3 nm lines equivalent widths in case `b)` first decline very slowly and at the height about 0.07 $R_\odot$ start to rise steeply. At the height above 0.08 $R_\odot$ they reach their maximum whose value is 3.5 – 22.5 times larger than maximum value of equivalent width of case `a)`. After this peak equivalent widths decline with height first rapidly and from height 0.1 $R_\odot$ more slowly as in case `a)`. The shape of the equivalent width relations for case `c)` are similar but they reach their maxima at lower heights (about 0.07 $R_\odot$) and values of these maxima are smaller than maxima of case `b)`. The peaks in equivalent width relations for cases `b)` and `c)` are due to considerably different values of electron density and temperature in area A as compared to area B.

For FeX 637.4 nm line all three equivalent width relations decline slowly up to height 0.1 $R_\odot$ and equivalent width of case `c)` is smaller than equivalent width of case a) and equivalent width of case `b)` is smaller than equivalent width of case `c)`. Only for this line the intensities for case without inhomogeneity are larger than intensities for cases `b)` and `c)`. It is because FeX is most abundant at temperature 1.0×10^6 K and temperature values in both areas of the inhomogeneity (for both model cases `b)` and `c)`) were considered much higher.

Equivalent widths of FeXV 705.86 nm line for both cases `b)` and `c)` decline from their maxima which are much higher than maximum of equivalent width of case `a)`. Equivalent widths of case `b)` are higher than equivalent widths in the case `c)`. Equivalent widths decline first slowly and at larger heights more

rapidly. For both FeX 637.4 nm and FeXV 705.86 nm, for heights larger than 0.1 $R_\odot$ all three equivalent width relations are the same.

4.2. Uncertainty in iron abundance determination

For almost all lines under study, intensities for cases `b)` and `c)` are larger, at heights from 1.05 $R_\odot$ up to 1.1 $R_\odot$ above limb, as compared to a purely spherically symmetrical case `a)`. If one tried to compute iron abundance from equivalent width relations for case `b)` or c) (Fig. 2) assuming spherical symmetry, such a value would be far from the iron abundance that we have adopted for our calculations. To show the difference, we computed iron abundance from equivalent width relations for cases `b)` and `c)` assuming spherically symmetrical distribution of spectral line intensity. For example from the equivalent width relation of FeXIV 530.3 nm line to height above the limb assuming spherical symmetry for case `b)` (Fig. 2) abundance of iron was computed using ionization and excitation equilibrium (Dzifčáková, 1998 and Dere et al., 1999 respectively). Those were the same data as for the line intensity computing. This iron abundance value was almost 86 times larger than the value of Fludra and Schmelz (1999), although spectral line intensities were computed exactly from this iron abundance. The abundance computed from FeXI 398.7 nm line for case `b)` was 7 times larger than value of Fludra and Schmelz (1999).

But for FeX 637.4 nm line the abundance of iron determined assuming spherical symmetry was lower than the value of Fludra and Schmelz (1999). For case `b)` it was 7 times and for case `c)` 2 times smaller.

It would be a problem to compute iron abundance from the emission line intensity relation to height above the limb using Pottasch's method in the presence of a coronal inhomogeneity. Pottasch presumed a monotonously declining relation and, as one can see, these relations are not monotonous in cases with inhomogeneity. So his method is rather imprecise and inapplicable for the solar corona above active regions when one wants to determine iron abundance from measurements of intensities of spectral lines there.

5. Suggested method for the iron abundance determination in presence of inhomogeneity

Method for the iron abundance determination by presence of coronal inhomogeneity at a place of emission spectral line measurement in solar corona is briefly outlined in this section.

Images, taken during the passage of an inhomogeneity across the solar disk, produced by the EIT/SoHO (Delaboudinière et al., 1995) in three wavelength bandpasses (171 Å with peak at 1.3×10^6 K, 195 Å at 1.6×10^6 K and 284 Å at 2.0×10^6 K) will be used for observing inhomogeneity from different sides and to find its 3-dimensional structure this way. Afterward it should be possible to construct its geometrical model (similar to those described in section 2).

Intensities of emission spectral lines (listed in section 3) of different iron ions will be measured above the limb at the place in the solar corona where the inhomogeneity is found after its passage across the solar disk. Intensities of each spectral line of interest should be measured in many different points of inhomogeneity. The term "different points" means, in this context, points of measurement in the solar corona with remarkably different intensities and physical conditions. Number of these points should be much larger than the predicted number of the areas in the inhomogeneity model.

First we will subtract contribution of the quiet corona from measured intensities. It is material in front of and behind the inhomogeneity. Intensities of spectral lines for the quiet corona will be measured in the vicinity of the coronal inhomogeneity where no other inhomogeneity ought to be present. After that, if functions $f(n_\mathrm{e}, T)$ and $g(T)$ for all spectral lines of interest are known (section 3), it will be possible to compute the iron abundance $A(\mathrm{Fe})$, temperature T and electron density n_e in all areas of the inhomogeneity model by minimizing function (least square method):

$$\Phi = \sum_i \left[I_i - \mathrm{C}_o \sum_{\mathrm{area}} A(\mathrm{Fe})\, G(n_\mathrm{e}, T)\, n_\mathrm{e}\, d_{\mathrm{area}} \right]^2 , \tag{3}$$

where $\sum_i$ means the sum of all measurements of intensity of given spectral line, I_i is the intensity measurement i with subtracted quiet corona contribution, $\sum_{\mathrm{area}}$ is the sum for sections of the line of sight in all separate areas of the inhomogeneity model. d_{area} is the length of the line of sight section in a given area of the inhomogeneity. The constant C_o substitutes the following formula:

$$\mathrm{C}_o = \frac{h\, c\, A_{ul}}{4\pi\, \lambda_o} \frac{N(H)}{n_\mathrm{e}} . \tag{4}$$

It is clear that there are not exactly separated areas with different electron densities and values of temperature in the inhomogeneity but physical conditions are changing continuously. But a more refined division of the inhomogeneity model on such areas will be used, the more realistic inhomogeneity description will be obtained. The best approximation of the inhomogeneity model to the observations could be made by minimization of Φ, obtaining electron density n_e, ionic temperature T and iron abundance $A(\mathrm{Fe})$ for each area of the inhomogeneity. Minimizing the function Φ is, in fact, the least square method problem with the unknowns n_e, T and $A(\mathrm{Fe})$ for each area of the inhomogeneity.

For applying suggested method to real data it is important to know how errors and noise in measurements of intensities of spectral lines could influence abundance, electron density and temperature values in every area of the inhomogeneity estimated by minimization of Φ (formula (3)). For that reason we adopted some artificial noise into the green coronal line intensity relations to height above the limb computed for our case `b)`.

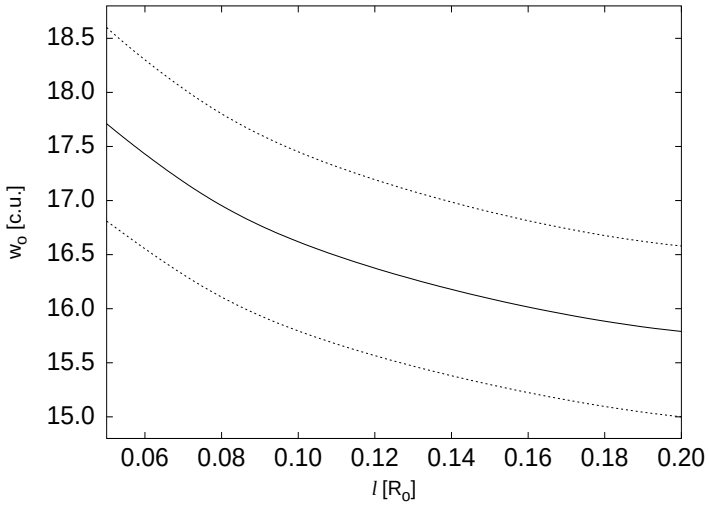

Figure 3. A green coronal spectral line intensity relation to height above the limb (solid curve) for the quiet corona (case `a)`). Dashed curves specify limits for errors of given accuracy $\pm 5\%$ for individual intensity measurements.

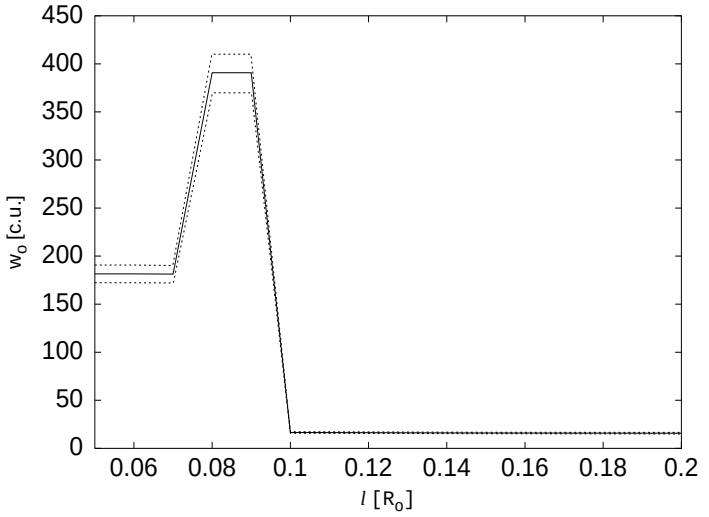

Figure 4. A green coronal spectral line intensity relation to height above the limb (solid curve) for the place in the solar corona where a box-shaped inhomogeneity (case `b)`) is present. Dashed curves specify limits for errors of given accuracy $\pm 5\%$ for individual intensity measurements.

For example, accuracy of the photographic photometry by ideal conditions (good weather during observation, good quality of optics and good adjustment of the observing instrument and microphotometer, etc.) is maximally ±5 %. We used this accuracy as an example for our noise modeling. We have taken green coronal line intensity relation for model `a` (figure 1 a)) as quiet corona intensity relation to height above the limb. By analogy, we have taken intensity of green coronal line relation for case `b)` (figure 1 b)) as the intensity relation to height above the limb at position in the solar corona where the inhomogeneity is located. These two relations are drawn by solid curve in figures 3. and 4. Borders (given by an accuracy ±5 %) for errors of " measurements " from real values of intensity for both relations are drawn by dashed curves in the same graphs.

We used following extreme cases for guesses of possible errors for estimates of values of abundance, electron density and electron temperature for every area of inhomogeneity due to errors in intensity measurements:
1) Higher by 5 % (than model values) values of intensity of the green coronal line measured at position in the solar corona where the inhomogeneity is located and lower by 5 % (than model values) values of intensity measured in the quiet corona. Such a case would lead to overestimate of abundance by 9 % or to overestimate of electron density by 5 % in area A of inhomogeneity. In area B it would lead to overestimate of abundance by 55 % or to overestimate of electron density by 55 % or to underestimate of electron temperature by 3 %.

2) In the opposite case (lower by 5 % values of intensity measured at position of inhomogeneity location and higher by 5 % values of intensity measured in quiet corona) it would lead to abundance underestimate by 1.5 % or to underestimate of electron density by 0.9 % in area A. It would also lead to overestimate of abundance by 0.5 % or to underestimate by 6.8 % of electron temperature by 6.8 % in area A. In area B it would lead to overestimate of abundance by 25 % or to overestimate of electron density by 138 % or to electron temperature underestimate by 1.4 %.

In practice, when one would be applying our method to real data, uncertainties in estimations of all three parameters (abundance, electron density, ionic temperature) for all areas of geometrical three-dimensional inhomogeneity model could be guessed as follows. First, the values of all three parameters would be estimated for every area of a three-dimensional geometrical model of the inhomogeneity using minimization formula (3). After that, values of parameters for all areas of the three-dimensional geometrical inhomogeneity model could be changed (both by decreasing and increasing them) only so much that computed values of intensity would correspond to measured ones. Then differences between original and changed values of parameters are possible uncertainties in estimation of those parameters.

It is obvious that errors in intensity measurement could remarkably influence estimation of physical parameters for individual areas of inhomogeneity.

Further, it is possible that errors in estimations of physical parameters from real values in one area of inhomogeneity are dependent on errors of estimations of physical parameters in the other area. Even error in estimation of one physical parameter in some area of inhomogeneity can influence precision of estimate of other physical parameters in the same area of inhomogeneity. We recommend to use not only intensities of spectral lines in minimization formula (3) but ratios of intensities of spectral lines too. This is useful for eliminating over- or under-estimates of physical parameters and ambiguity of temperature estimates. For example some ratios of intensities of spectral lines of the same ion in the same spectral range are suitable for the electron density estimates. And some ratios of intensities of spectral lines of different ions of the same element are suitable for temperature estimates. It is important for states of ionization of those ions to be close one to another. Such ratios of intensities of spectral lines are hard to measure in the visible range of spectrum. A lot of spectral lines of many different iron ions are, however, observed in the EUV range of spectrum by CDS/SoHO.

6. Discussion

Spectral lines intensities found from our models for height 0.05 $R_\odot$ above limb can be compared with the observed ones. These intensities resulted are only theoretical and the observed intensities could be assumed as reference showing whether our models are realistic. Pottasch (1963) used observations made both during and except of the total solar eclipses in years 1949 – 1954, especially during total eclipse in February 25, 1952. Equivalent width estimated by him for 530.3 nm FeXIV line at height 0.05 $R_\odot$ above limb was 48.64 c.u.; it is almost 4 times less than the intensity of our model for case `b)` at the same height and 1.4 times less than our intensity for case `c)`. For 637.4 nm FeX line value of Pottasch (1963) was much larger (difference about 3 orders of magnitude) than that computed from our theoretical models. It would be so because there was no area with temperature 1.0×10^6 K in our inhomogeneity model by which FeX abundance reaches its maximum. Therefore the equivalent width for this spectral line estimated by Pottash is much larger than the value computed from our model.

Equivalent widths for FeXIV 530.3 nm and FeXV 705 nm lines resulting from our theoretical model for case `b)` agree well with those of Magnant-Crifo (1973). He has used observations made during the total solar eclipse on May 30, 1965. Those observations were made at the place in solar corona where a coronal condensation was present. Equivalent widths of FeX 637.4 nm and FeXI 398.7 nm lines estimated by him are more different from values computed using our theoretical models (especially for first line the value computed by us is about 1000 times smaller). It is because our model did not contain any area with temperature about 1.0×10^6 K where FeX and FeXI ions would reach larger concentrations.

In practice it will be needed to take a more realistic model of the inhomogeneity with more than two areas and with inhomogeneous temperature changed from 0.5×10^6 K where there are more abundant ions at lower ionization state, to 5.0×10^6 K where are more abundant ions at higher state, especially FeXV. But our models b) and c) are sufficient for illustration that even small areas in solar corona with different value of electron density and temperatures comparing to surrounding corona can have large influence on spectral lines intensity.

7. Conclusions

When there is some inhomogeneity in the solar corona in the place where intensities of spectral lines of different iron ions are measured, one could obtain unreal iron abundance value without taking influence of this inhomogeneity into account. This is due to large differences in spectral lines intensities for the cases with and without inhomogeneity.

Given emission spectral line intensity relation to height above the limb need not to be monotonous and exponentially declining. There can exist some peaks due to suitable physical conditions (especially temperature and electron density) for this spectral line radiation in some areas of the inhomogeneity. We computed relations of coronal emission spectral line equivalent width to height above the limb for one model without any inhomogeneity (case `a)`) and two models with different shapes of inhomogeneity (cases `b)`, `c)`) and we showed that intensities relations for case with and without inhomogeneity could differ one from another. Equivalent width relations to height above the limb are not monotonously declining and that is why method developed and used by Pottasch (1963) (assuming solar corona as spherically symmetrical) cannot be used.

That is why the iron abundance determinations having neglected a fine structure of the solar corona are unrealistic except for the quiet corona and coronal holes. Observations of several visible emission spectral lines of iron ions in the same place in the solar corona, needed for reliable iron abundance determination, is possible only in place where an inhomogeneity is present (mainly above an active region). But in such places in the solar corona the assumption of spherical symmetry cannot be used. In the quiet corona, where spherical symmetry could be used, intensities of many spectral lines (except for the green and red ones) are not measurable.

A new method for the iron abundance determination in the solar corona suggested by us (using minimizing of differences between theoretical and measured intensities) would overcome the problem of inhomogeneous structure of the solar corona.

Acknowledgements. This work was supported by Grant Agency for Science of Slovak Academy of Sciences (grant No. 5017/98).

References

Anders, E., Grevesse, N.: 1989, *Geochim. Cosmochim. Acta* **53**, 197
Delaboudinière, J.-P., Artzner, G.E., Brunaud, J., Gabriel, A.H., Hochedes, J.F., Millier, F., Song, X.Y., Au, B., Dere, K.P., Howard, R.A., Kreplin, R., Michels, D.J., Moses, J.D., Defise, J.M., Jamar, C., Rochus, P., Chauvineau, J.P., Marioge, J.P., Catura, R.C., Lemen, J.R., Shing, L., Stern, R.A., Gurman, J.B., Neupert, W.M., Maucherat, A., Clette, F., Cugnon, P., Van Dessel, E.L.: 1995, *Sol. Phys.* **162**, 291
Doschek, G.A., Warren, H.P., Laming, J.M., Mariska, J.T., Wilhelm, K., Lemaire, P., Schühle, U., Moran, T.G.: 1997, *Astrophys. J., Lett.* **482**, L109
Dzifčáková, E.: 1998, *Sol. Phys.* **178**, 317
Feldman, U.: 1992, *Physica Scripta* **46**, 202
Fludra, A., Schmelz, J.T.: 1999, *Astron. Astrophys.* **348**, 286
Goldberg, L., Muller, E., Aller, L.H.: 1960, *Astrophys. J., Suppl. Ser.* **5**, 1
Grevesse, N., Sauval, A.J.: 1999, *Astron. Astrophys.* **347**, 348
Landi, E., Landini, M.: 1997, *Astron. Astrophys.* **327**, 1230
Landi, E., Landini, M., Dere, K.P., Young, P.R., Mason, H.E.: 1999, *Astron. Astrophys., Suppl. Ser.* **135**, 339
Magnant-Crifo, F.: 1973, *Sol. Phys.* **31**, 91
Mason, H.E.: 1975, *Mon. Not. R. Astron. Soc.* **171**, 119
Mason, H.E., Landi, E., Pike, C.D., Young, P.R.: 1999, *Sol. Phys.* **189**, 129
Meyer, J.-P.: 1991, *Adv. Space Res.* **11**, 269
Meyer, J.-P.: 1996, in *The Sun and Beyond*, eds.: J. Tran Thanh Van, L.M. Celnikier, H.C. Trung and S. Vauclair, Editions Frontières, Gif-sur-Yvette, 27
Neckel, H., Labs, D.: 1984, *Sol. Phys.* **90**, 205
Neckel, H., Labs, D.: 1985, *Sol. Phys.* **95**, 229
Peter, H.: 1998a, *Astron. Astrophys.* **335**, 691
Peter, H.: 1998b, *Space Sci. Rev.* **85**, 253
Philips, K.H.J., Pike, C.D., Lang, J., Watanbe, T., Takahashi, M.: 1994, *Astrophys. J.* **435**, 888
Pottasch, S.R.: 1963, *Mon. Not. R. Astron. Soc.* **125**, 543